The Society of Naval Architects of Japan

Computation of Ship's Resistance Using an NS Solver with Global Conservation

——Flat Plate and Series 60 (C_B=0.6) Hull——

by Yoshiaki Kodama

Summary

A globally conservative NS solver for flow past a ship hull has been developed. It uses a 3rd-order accurate upwind differencing of the preprocessing (MUSCL) type for inviscid terms, in which the non-uniformity of grid spacing is taken into account. Using the solver, the drag of a flat plate at zero incidence was computed in the Reynolds number range $R_e=4.0\times10^5$ to $R_e=4.0\times10^7$. The dependence of the drag on the degree of clustering of grid points was checked. The computed drag agreed with the Schoenherr value within 4%. An appropriate criterion for the minimum grid spacing $\Delta_{\min}$ adjacent to solid wall with this particular scheme seems to be $\Delta_{\min}=0.005/\sqrt{R_e}$.

Then the drag of the Series 60 ($C_B=0.6$) ship hull with the double model assumption was computed in the same Reynolds number range using grids with various $\Delta_{\min}$ and various degree of clustering toward bow and stern. Although the computed drag values showed some scattering among different grids, the results with the smallest $\Delta_{\min}$ agreed well with the measured values throughout the Reynolds number range.

1. Introduction

Accurate estimation of ship's drag (resistance) is very important from the propulsive performance point of view. Since ship's drag is generated through viscous and inviscid interactions, neither the powerful potential theory nor the boundary-layer theory can estimate the drag accurately by itself. NS solvers, i. e. CFD, which contain the above two theories as subsets, seem to be the only means that can achieve this goal.

CFD (Computation Fluid Dynamics) has been making remarkable progress, and its field of application is quite wide already. Since CFD can provide detailed information of flowfields, it is particularly useful in obtaining qualitative information such as flow structures. However, using CFD, to obtain macroscopic or integrated information such as lift or drag acting on a body in flow is difficult. Especially, accurate computation of the drag of a streamlined body like a ship hull is difficult, partly because the pressure drag component comes out as a small difference between the large two at bow and stern.

One of the major sources of the difficulty is the ambiguity in the way the drag is computed. A drag value may depend on the integration path it takes, or on the way the surface shear stress is computed. In order to remove this ambiguity, the author proposed an NS solver with global conservation[1),2),3),4)]. The word "global conservation" means that the conservation property is satisfied everywhere in the computed flow domain, all the way down to boundaries. The global conservation property automatically assures that computed macroscopic forces such as lift and drag do not depend on the integration path, i. e., the forces are unique. In the globally conservative scheme, there is no ambiguity in the way the surface stress terms are estimated, since it is made fully consistent with the solver itself.

Using the solver, the drag of a two-dimensional circular cylinder was computed at the Reynolds number R_e=40, and the computed drag agreed well with other well-established computed values[1)]. The scheme was extended to three dimensions, and the flow past a Series 60 (C_B=0.60) ship hull was computed[3)]. In the Reynolds number range $R_e=3.0\times10^6$ to 4.0×10^6, the computed drag agreed well with the measured values. However, in computing the drag of the same ship in the range $R_e=4.0\times10^5$ to 4.0×10^7, the computed drag tended to deviate systematically toward higher values from the measurements[4)] at higher Reynolds number range.

The present work shows an effort to clarify the cause of the deviation and to compute the drag more accurately. The drag of the same ship is computed using grids with various degree of clustering. The drag of a flat plate is also computed, since the flow around it has

* Ship Research Institute

Received 9th July 1992
Read at the Autumn meeting 9, 10 Nov. 1992

NII-Electronic Library Service

The Society of Naval Architects of Japan

much similarity with that of the Series 60 ($C_B=0.60$) hull, which is very fine.

In the present work, the scheme is modified such that the third-order accuracy in computing the inviscid terms is maintained under non-uniform grid spacing, while the previous scheme had third-order accuracy only if the grid spacing is uniform. In contrast to the postprocessing approach adopted in the previous works, the present scheme adopts the preprocessing (MUSCL) approach[7] in constructing the third-order accurate upwind differencing, because the non-uniformity of the grid spacing is much more easily taken into account there.

In the computation, the free surface is treated as the plane of symmetry, i. e. the double model flow assumption.

2. Formulation

2.1 Discretization of Governing Equations

The nondimensionalized Navier-Stokes equations, i. e. the conservation of x-, y-, z- momentum, and mass, are written in conservation form as

$$\frac{\partial q}{\partial t}+\frac{\partial F}{\partial x}+\frac{\partial G}{\partial y}+\frac{\partial H}{\partial z}+\frac{\partial F_v}{\partial x}+\frac{\partial G_v}{\partial y}+\frac{\partial H_v}{\partial z}=0 \quad (1)$$

where

$$q=\begin{bmatrix}u\\v\\w\\p\end{bmatrix},\ F=\begin{bmatrix}u^2+p\\uv\\uw\\\beta u\end{bmatrix},\ G=\begin{bmatrix}vu\\v^2+p\\vw\\\beta v\end{bmatrix},\ H=\begin{bmatrix}wu\\wv\\w^2+p\\\beta w\end{bmatrix},$$

$$F_v=-\nu\begin{bmatrix}\tau'_{xx}\\\tau'_{xy}\\\tau'_{xz}\\0\end{bmatrix},\ G_v=-\nu\begin{bmatrix}\tau'_{xy}\\\tau'_{yy}\\\tau'_{yz}\\0\end{bmatrix},\ H_v=-\nu\begin{bmatrix}\tau'_{xz}\\\tau'_{yz}\\\tau'_{zz}\\0\end{bmatrix}, \quad (2)$$

$$\nu=\frac{1}{R_e}+\nu_t$$

$$\begin{cases}\tau'_{xx}=2u_x,\ \tau'_{xy}=u_y+v_x,\ \tau'_{xz}=u_z+w_x,\\ \tau'_{yy}=2v_y,\ \tau'_{yz}=v_z+w_y,\\ \tau'_{zz}=2w_z\end{cases} \quad (3)$$

In the equation for mass conservation, i. e. the fourth component of eq. (1), pseudocompressibility is introduced with a positive constant β. ν_t is the kinematic eddy viscosity.

As shown in Fig. 1, the cell-centered layout is adopted. Flow variable nodes are placed at the center of grid cells, and the grid cells are used as control volumes. Fig. 1(a) shows the 2D case, and (b) shows the 3D case, i. e., the present case.

The finite volume integration is used for discretization. In order to derive the discretized equations for the flow variables at (i, j, k), the governing equations are integrated at the grid cell including the point (i, j, k).

$$\iiint_{V_{i,j,k}}\left(\frac{\partial q}{\partial t}+\frac{\partial F}{\partial x}+\frac{\partial G}{\partial y}+\frac{\partial H}{\partial z}+\frac{\partial F_v}{\partial x}+\frac{\partial G_v}{\partial y}+\frac{\partial H_v}{\partial z}\right)dV=0 \quad (4)$$

The first term of the above equation is approximated as the volume of the cell times the $\partial q/\partial t$ value at (i, j, k),

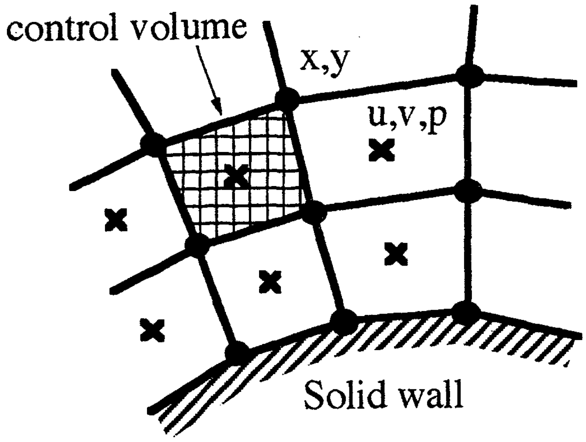

(a) 2D case

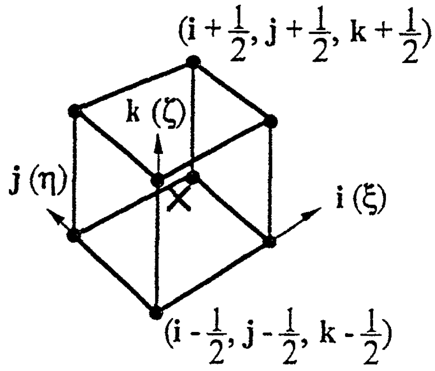

(b) 3D case

Fig. 1 Cell-centered layout and control volume

the cell center. That is

$$\iiint_{V_{i,j,k}}\frac{\partial q}{\partial t}dV\simeq V_{i,j,k}\frac{\partial q}{\partial t}_{i,j,k} \quad (5)$$

where the volume is computed as the sum of six tetrahedra[6].

In order to discretize the other terms, the Gauss integral theorem is used

$$\iiint_V \mathrm{grad}\,\phi dV=\iint_S \phi \boldsymbol{n}^* dS, \quad (6)$$

where $\boldsymbol{n}^*=(n_x^*, n_y^*, n_z^*)$ is a unit outward normal vector. The above theorem is applied to eq. (4), and the surface integration of the hexahedron is divided into six quadrilateral surfaces as

$$\begin{aligned}\iiint_V \frac{\partial F}{\partial x}dV=&\iint_S F n_x^* dS\\ \simeq&\{F(Sn_x)^\xi\}_{i+\frac{1}{2},j,k}-\{F(Sn_x)^\xi\}_{i-\frac{1}{2},j,k}\\ &+\{F(Sn_x)^\eta\}_{i,j+\frac{1}{2},k}-\{F(Sn_x)^\eta\}_{i,j-\frac{1}{2},k}\\ &+\{F(Sn_x)^\zeta\}_{i,j,k+\frac{1}{2}}-\{F(Sn_x)^\zeta\}_{i,j,k-\frac{1}{2}}\end{aligned} \quad (7)$$

where (i, j, k) are the numbering in ξ-, η-, and ζ-directions. The negative signs in the last equality come from the definition of the unit normal vector $\boldsymbol{n}$, which is always in the positive ξ-, η, or ζ-direction. $(Sn_x)^\xi_{i+\frac{1}{2},j,k}$, the area of the $i+\frac{1}{2}$ surface projected in the x-axis direction, is computed using the area formula for a

NII-Electronic Library Service

The Society of Naval Architects of Japan

quadrilateral shown below.

$$(Sn_x)^{\xi}_{i+\frac{1}{2},j,k}=\frac{1}{2}[(y_2-y_4)(z_3-z_1)-(z_2-z_4)(y_3-y_1)] \quad (8)$$

where

$$\begin{cases} P_1\equiv P_{i+\frac{1}{2},j-\frac{1}{2},k-\frac{1}{2}}, & P_2\equiv P_{i+\frac{1}{2},j+\frac{1}{2},k-\frac{1}{2}} \\ P_3\equiv P_{i+\frac{1}{2},j+\frac{1}{2},k+\frac{1}{2}}, & P_4\equiv P_{i+\frac{1}{2},j-\frac{1}{2},k+\frac{1}{2}} \end{cases}$$

Note that, using the above formula, the projected area of a closed body surface, which is divided into many quadrilaterals, exactly sums to zero. This property should be called "the conservation of projected areas". This automatically assures that the integrated pressure drag component of a closed body is exactly zero if the pressure is constant everywhere.

The other terms in eq. (4) are treated similary, and the discretized governing equation shown below is derived.

$$\begin{aligned} V_{i,j,k}\frac{\partial q}{\partial t_{i,j,k}}&+(\hat{F}+\hat{F}_v)_{i+\frac{1}{2}}-(\hat{F}+\hat{F}_v)_{i-\frac{1}{2}} \\ &+(\hat{G}+\hat{G}_v)_{j+\frac{1}{2}}-(\hat{G}+\hat{G}_v)_{j-\frac{1}{2}} \\ &+(\hat{H}+\hat{H}_v)_{k+\frac{1}{2}}-(\hat{H}+\hat{H}_v)_{k-\frac{1}{2}}=0 \end{aligned} \quad (9)$$

where, for example, $(\ )_{i+\frac{1}{2}}$ means $(\ )_{i+\frac{1}{2},j,k}$ and

$$\begin{cases} \hat{F}=(Sn_x)^{\xi}F+(Sn_y)^{\xi}G+(Sn_z)^{\xi}H \\ \hat{G}=(Sn_x)^{\eta}F+(Sn_y)^{\eta}G+(Sn_z)^{\eta}H \\ \hat{H}=(Sn_x)^{\zeta}F+(Sn_y)^{\zeta}G+(Sn_z)^{\zeta}H \end{cases} \quad (10)$$

and similarly with $\hat{F}_v$, $\hat{G}_v$, and $\hat{H}_v$.

2.2 Inviscid terms

The value of the inviscid terms at each cell face is computed using the third-order accurate upwind differencing constructed within the flux-difference splitting framework. The third-order accuracy is attained in the preprocessing (MUSCL) manner [7], in which the nonuniformity of grid spacings is taken into account. The reason that the preprocessing approach has been adopted here, in contrast to the postprocessing approach adopted in the previous reports, is that high-order accuracy under the nonuniform grid spacing is much more easily attained using the preprocessig approach.

As a building block, a flux difference a the cell face $i+\frac{1}{2}$ is defined as a function of q at the left and right side of the cell face, and the metric (i. e. projected area) terms.

$$\begin{aligned} \delta\hat{F}_{i+\frac{1}{2}}&=\hat{F}(q^R_{i+\frac{1}{2}}, Sn^{\xi}_{i+\frac{1}{2}})-\hat{F}(q^L_{i+\frac{1}{2}}, Sn^{\xi}_{i+\frac{1}{2}}) \\ &=A^{LR}_{i+\frac{1}{2}}\delta q^{LR}_{i+\frac{1}{2}} \end{aligned} \quad (11)$$

where

$$\begin{cases} A^{LR}_{i+\frac{1}{2}}=A(q^{LR}_{i+\frac{1}{2}}, Sn^{\xi}_{i+\frac{1}{2}}) \\ A(q, Sn)=S\begin{bmatrix} U+un_x, & un_y, & un_z, & n_x \\ vn_x, & U+vn_y, & vn_z, & n_y \\ wn_x, & wn_y, & U+wn_z, & n_z \\ \beta n_x, & \beta n_y, & \beta n_z, & 0 \end{bmatrix} \\ U=un_x+vn_y+wn_z \\ q^{LR}_{i+\frac{1}{2}}=\frac{1}{2}(q^L_{i+\frac{1}{2}}+q^R_{i+\frac{1}{2}}) \\ \delta q^{LR}_{i+\frac{1}{2}}=q^R_{i+\frac{1}{2}}-q^L_{i+\frac{1}{2}} \end{cases} \quad (12)$$

The flux difference is divided into positive and negative components depending on the signs of the eigenvalues[3] as

$$\delta\hat{F}=\delta\hat{F}^{+}+\delta\hat{F}^{-} \quad \text{where} \quad \delta\hat{F}^{\pm}=A^{\pm}\delta q. \quad (13)$$

Then the inviscid flux at $i\pm\frac{1}{2}$ is defined as

$$\begin{cases} \hat{F}_{i+\frac{1}{2}}=\hat{F}(q^L_{i+\frac{1}{2}}, Sn^{\xi}_{i+\frac{1}{2}})+\delta\hat{F}^{-}_{i+\frac{1}{2}} \\ \hat{F}_{i-\frac{1}{2}}=\hat{F}(q^R_{i-\frac{1}{2}}, Sn^{\xi}_{i-\frac{1}{2}})-\delta\hat{F}^{+}_{i-\frac{1}{2}} \end{cases} \quad (14)$$

Substituting $i+1$ into i in the lower half of the above equation, and equating it with the upper half produces eq. (13), which means that the present scheme is conservative.

The q^L and q^R are determined in an upwind differencing manner. It is explained using 1D case for simplicity. In approximating a first derivative with a constant coefficient c as shown below

$$c\frac{\delta q}{\delta\xi^*}=c\frac{q_{i+\frac{1}{2}}-q_{i-\frac{1}{2}}}{\Delta\xi^*}, \quad (15)$$

$q_{i+\frac{1}{2}}$ is determined depending on the sign of c.

$$\begin{aligned} q_{i+\frac{1}{2}}&=q^L_{i+\frac{1}{2}} \quad (c>0) \\ &=q^R_{i+\frac{1}{2}} \quad (c<0) \end{aligned} \quad (16)$$

That is, when the signal propagates from left to right, $q^L_{i+\frac{1}{2}}$ is used as $q_{i+\frac{1}{2}}$ and vice versa.

<u>1st-order accurate upwind differencing</u>

As shown in Fig. 2, zero extrapolation is used for defining q^L and q^R.

$$\begin{cases} q^L_{i+\frac{1}{2}}=q_i \\ q^R_{i+\frac{1}{2}}=q_{i+1} \end{cases} \quad (17)$$

The substitution of the above equation into eq. (15) produces the 1st-order accurate upwind differencing about the point i.

<u>2nd-order accurate upwind differencing with uniform grid spacing</u>

Assuming all Δ_i in Fig. 2 are constant, linear extrapolation is used.

$$\begin{cases} q^L_{i+\frac{1}{2}}=\frac{3}{2}q_i-\frac{1}{2}q_{i-1} \\ q^R_{i+\frac{1}{2}}=\frac{3}{2}q_{i+1}-\frac{1}{2}q_{i+2} \end{cases} \quad (18)$$

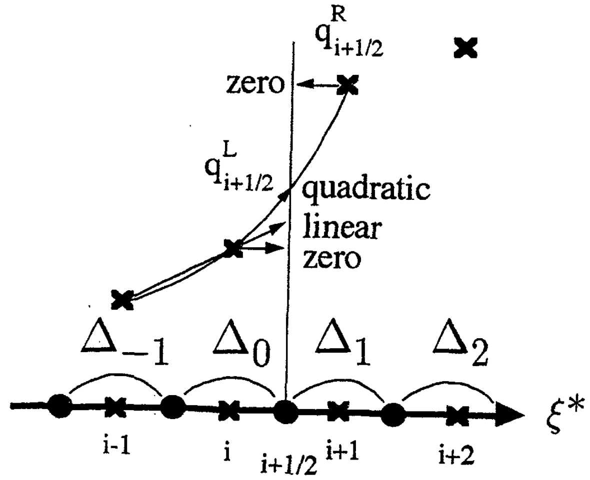

Fig. 2 $2q^L_{i+\frac{1}{2}}$ and $q^R_{i+\frac{1}{2}}$ for upwind differencing

NII-Electronic Library Service

The Society of Naval Architects of Japan

QUICK scheme with uniform grid spacing

Assuming constant Δ_i again, quadratic interpolation is used.

$$\begin{cases} q^L_{i+\frac{1}{2}}=\frac{3}{8}q_{i+1}+\frac{6}{8}q_i-\frac{1}{8}q_{i-1} \\ q^R_{i+\frac{1}{2}}=\frac{3}{8}q_i+\frac{6}{8}q_{i+1}-\frac{1}{8}q_{i+2}. \end{cases} \tag{19}$$

The substitution of the above equation into eq. (15) does not produce the 3rd-order but the 2nd-order accurate upwind differencing. It is usually called the QUICK scheme.

3rd-order accurate upwind differencing with uniform grid spacing (U)

Using the Taylor series expansion about the point i, the following interpolation formula which leads to the 3rd-order accurate upwind differencing is derived.

$$\begin{cases} q^L_{i+\frac{1}{2}}=\frac{2}{6}q_{i+1}+\frac{5}{6}q_i-\frac{1}{6}q_{i-1} \\ \quad =q_i+\Phi_1\delta q_{i-\frac{1}{2}}+\Phi_2\delta q_{i+\frac{1}{2}} \\ q^R_{i+\frac{1}{2}}=\frac{2}{6}q_i+\frac{5}{6}q_{i+1}-\frac{1}{6}q_{i+2} \\ \quad =q_i+(1-\Phi_2)\delta q_{i+\frac{1}{2}}-\Phi_1\delta q_{i+\frac{3}{2}} \end{cases} \tag{20}$$

where

$$\Phi_1=\frac{1}{6},\ \Phi_2=\frac{1}{3}\quad \delta q_{i+\frac{1}{2}}=q_{i+1}-q_i,\cdots \tag{21}$$

This differencing will be called the upwind differencing U (the letter for "uniform").

3rd-order accurate upwind differencing with non-uniform grid spacing (NU)

Following Sawada[8], in case the grid spacing is not uniform, as shown in Fig. 2, $q(\xi^*)$, the value of q as a function of the real length ξ^*, is assumed to be quadratic.

$$q(\xi^*)=a\xi^{*2}+b\xi^*+c \tag{22}$$

Since the location of each cell center is unknown in this case, the curve fitting in the integrated sense is used in the three consequtive intervals.

$$q_{i+m}=\frac{1}{\Delta_m}\int_{\xi^*_{i+m-\frac{1}{2}}}^{\xi^*_{i+m+\frac{1}{2}}} q(\xi^*)d\xi^* \quad (m=-1,0,1) \tag{23}$$

Then the value of $q^L_{i+\frac{1}{2}}$ is determined as $q(\xi^*_{i+\frac{1}{2}})$, and similarly with $q^R_{i+\frac{1}{2}}$.

$$\begin{cases} q^L_{i+\frac{1}{2}}=q_i+\Phi^L_1\delta q_{i-\frac{1}{2}}+\Phi^L_2\delta q_{i+\frac{1}{2}} \\ q^R_{i+\frac{1}{2}}=q_i+(1-\Phi^R_2)\delta q_{i+\frac{1}{2}}-\Phi^R_1\delta q_{i+\frac{3}{2}} \end{cases} \tag{24}$$

where

$$\begin{cases} \Phi^L_1=\dfrac{\Delta_0\Delta_1}{(\Delta_{-1}+\Delta_0+\Delta_1)(\Delta_{-1}+\Delta_0)} \\ \Phi^L_2=\dfrac{\Delta_0(\Delta_{-1}+\Delta_0)}{(\Delta_{-1}+\Delta_0+\Delta_1)(\Delta_0+\Delta_1)} \\ \Phi^R_1=\dfrac{\Delta_0\Delta_1}{(\Delta_0+\Delta_1+\Delta_2)(\Delta_1+\Delta_2)} \\ \Phi^R_2=\dfrac{\Delta_1(\Delta_1+\Delta_2)}{(\Delta_0+\Delta_1+\Delta_2)(\Delta_0+\Delta_1)} \end{cases}$$

The above equations satisfy the requirement that when the grid spacing is uniform, they reduce to eqs. (20) and (21). Sawada[8] gives a slightly different definition of $q^L_{i+\frac{1}{2}}$, which does not satisfy the requirement. It is interesting that, as in the above equation, the quadratic curve fitting in the integrated sense produces the 3rd-order accurate formula, but the curve fitting in the collocated sense, i. e. QUICK, fails to do so. This differencing will be called the upwind differencing NU (the letters for "non-uniform").

It is straightforward to extend this formula to the 3D case, in which the grid spacing is computed by taking the average of the four corner points at each cell face. Fig. 3 shows an example of computed results. Fig. 3(a) shows a grid around a ship hull, in which the grid points $k=5$ (k is the number in ζ-direction, with $k=1$ being at solid wall) is relocated by linear interpolation toward the $k=4$ points with the new distance between $k=4$ and $k=5$ being only 1% of the original value. The arrows in the figure shows its location. Fig. 3(b) shows the pressure contours obtained using the upwind differencing U. Fig. 3(c) shows a similar result using the upwind differencing NU. Comparing the two figures, it is evident that the differencing NU produces a result better than the differencing U when the grid spacing is not uniform.

It should be noted that the differencing NU does not

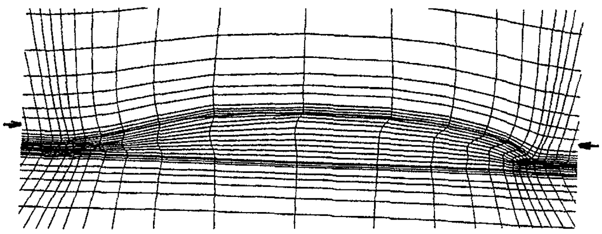

Fig. 3(a) Grid with sudden change in ζ-spacing at $k=5$ (arrows).

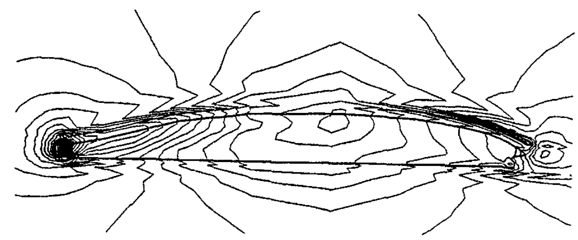

Fig. 3(b) Pressure contours by the upwind differencing U. $Re=10^4$, $\Delta C_p=0.02$.

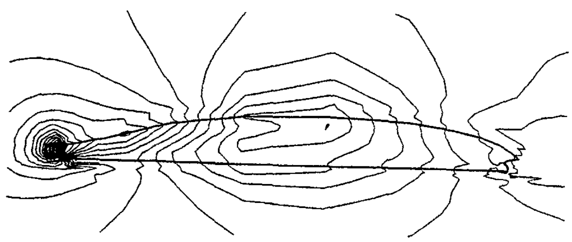

Fig. 3(c) Pressure contours by the upwind differencing NU. $Re=10^4$, $\Delta C_p=0.02$.

NII-Electronic Library Service

The Society of Naval Architects of Japan

remedy the adverse effect of grid singularities such as kinks and skewness.

On the solid wall surface, the flux value is computed directly by substituting $u=v=w=0$ and pressure p being made equal to that at the cell center, i. e., zero extrapolation by half the grid cell length

2.3 Viscous terms

The Gauss integral theorem eq. (6) is used in determining the first derivatives of velocity components. For example, u_x at the cell face $(i, j, k+(1/2))$ is determined by taking the volume of integration $V_{i,j,k+\frac{1}{2}}$ which is shown as $V_{\rm II}$ wih $k=1$ in Fig. 4.

$$u_{x i,j,k+\frac{1}{2}}=\frac{1}{V_{i,j,k+\frac{1}{2}}}(u_E\{Sn_x\}_E-u_W\{Sn_x\}_W +u_N\{Sn_x\}_N-u_S\{Sn_x\}_S +u_T\{Sn_x\}_T-u_B\{Sn_x\}_B) \qquad (25)$$

where

$$\begin{cases} u_E=u_{i,j,k+1} \\ u_W=u_{i,j,k} \\ u_N=\frac{1}{4}(u_{i+1,j,k+1}+u_{i,j,k+1}+u_{i+1,j,k}+u_{i,j,k}) \\ u_S=\frac{1}{4}(u_{i,j,k+1}+u_{i-1,j,k+1}+u_{i,j,k}+u_{i-1,j,k}) \\ u_T=\frac{1}{4}(u_{i,j+1,k+1}+u_{i,j,k+1}+u_{i,j+1,k}+u_{i,j,k}) \\ u_B=\frac{1}{4}(u_{i,j,k+1}+u_{i,j-1,k+1}+u_{i,j,k}+u_{i,j-1,k}) \end{cases}$$

Note that the above equation is formally 2nd-order accurate, i. e. 2nd-order accurate on uniform grids.

At the solid wall ($k=\frac{1}{2}$), using the two integration volumes $V_{\rm I}$ and $V_{\rm II}$ shown in Fig. 4, $u_{xk=3/4}$ and $u_{xk=3/2}$ are determined

$$\int_{V{\rm I}} u_x dV \rightarrow u_{x3/4} \qquad \int_{V{\rm II}} u_x dV \rightarrow u_{x3/2}$$

Then the u_x at the solid wall is determined in the following two ways.

<u>1st-order accuracy (zero extrapolation)</u>

$$u_{x\frac{1}{2}} \doteqdot u_{x\frac{3}{4}} \qquad (2.3.2)$$

The scheme which uses this equation will be called V1, i. e. the viscous terms with 1st-order accuracy.

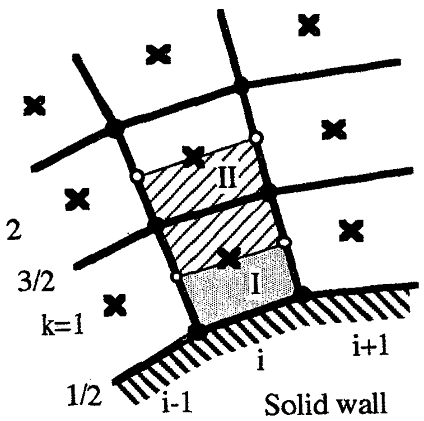

Fig. 4 Volume of Gauss integration for viscous terms near solid wall.

<u>2nd-order accuracy (linear extrapolation)</u>

$$u_{x\frac{1}{2}} \doteqdot \frac{4}{3}u_{x\frac{3}{4}}-\frac{1}{3}u_{x\frac{3}{2}} \qquad (2.3.3)$$

This will be called V2.

2.4 Eddy viscosity ν_t

The Baldwin-Lomax zero equation turbulence model is used. In most of the computation, smoothing is applied by averaging with the four neighboring points on the same k plane. The smoothing seems to increase the numerical stability. The cases in which the smoothing is applied will be called SM, and the cases without it will be called NSM.

2.5 Time integration

The Padé time diffencing form[3] is used for time integration with $\theta=1.0$, i. e. the Euler implicit. In the inviscid terms of the unsteady part, the 1st-order upwind differencing is used, by setting $\Phi_1=\Phi_2=0$. This does not affect the steady-state part, that is, the converged inviscid part has 3rd-order accuracy. The IAF procedure is adopted.

2.6 Boundary conditions

The bounday conditions are summarized in Table 1. At the upstream boundary, zero extrapolation is used for pressure. In case the uniform flow condition, i. e. $p=0$, is used, a slight pressure jump occurs at the boundary. Therefore the zero extrapolation condition has been adopted.

3. Flat plate with zero attack angle

The grids for flat plate computation were generated analytically with H-grid topology. They are similar to those used in ref. 9). Table 2 shows the parameters for the grid generation. IM is the number of grid point in the streamwise direction. I_{FP} is the point number at the leading edge, I_{AP} is that at the trailing edge. KM is the

Table 1 Boundary conditions

Boundary	u,v,w	p
Upstream	u=1, v=w=0	zero extrapolation
Downstream	zero extrapolation	p=0
Left & Right	symmetry	symmetry
Top	u=1, v=w=0	p=0
Bottom	u=v=w=0	zero extrapolation

Table 2 Computed drag of a flat plate.
Part 1...minimum spacings.
Parameters: IM=81, KM=41, $I_{FP}=16$, $I_{AP}=60$, $R_{\rm outer}=1.0$,
$x_{\rm up}=-0.5$, $x_{\rm down}=2.0$, $\gamma_{c1}=0.3$,
$\beta=1.0$, NU, V2, SM, $\Delta t=0.1$.

Grid	R_e / $\Delta_{\min}$	4×10^5 / $C_T\times10^2$ (δ)	4×10^6	4×10^7
A	2×10^{-5}	0.5182 (0.0126)	0.3379 (0.04)	0.2428 (0.126)
B	1×10^{-5}	0.5174 (0.0063)	0.3331 (0.02)	0.2685 (0.0632)
C	0.5×10^{-5}	0.5174 (0.0032)	0.3325 (0.01)	0.2528 (0.0316)
D	0.25×10^{-5}	—	0.3307 (0.005)	0.2391 (0.0158)
E	0.125×10^{-5}	—	0.3311 (0.0025)	0.2346 (0.0079)
	Schoenherr	0.5294	0.3423	0.2365

NII-Electronic Library Service

The Society of Naval Architects of Japan

number of grid points in z-direction, i. e. the normal-to-wall direction. X_{up} and X_{down} are the x-coordinates of the upstream and downstream boundaries, while those of the leading and trailing edges being 0.0 and 1.0, respectively. Δ_{min} is the minimum grid spacing adjacent to the solid wall. R_{outer} is the distance in the z-direction between the plate and the top boundary. In ship flows this parameter denotes the outer radius of the top boundary. γ_{cl} is the clustering ratio in the $x(i)$-direction. It is defined as the ratio of the x spacing (Δx) at FP or AP and the average spacing between FP and AP. δ is the parameter defined using the equation

$$\Delta_{min}=\frac{\delta}{\sqrt{Re}}$$

, a criterion frequently used to determine the minimum grid spacing with $\delta=0.05$ in the previous computations[2),3),4),9)].

The table also shows the computed C_T (total drag) values at various Reynolds numbers with various grids. In this case there is no pressure drag component C_{pres}, and therefore C_T contains only the frictional component C_{fric}. The grid expansion ratio in the z-direction is approximately 1.3. The computations were continued until the C_T value integrated on the plate agrees with that integrated at outer boundaries with sufficient accuracy, say up to four significant figures. The C_T values tend to converge as Δ_{min} decreases. The C_T values at $R_e=4.0\times10^7$ are plotted with Δ^2_{min} in the horizontal axis in Fig. 5. The values of the grids C, D, and E converge linearly, which suggests that the viscous term has 2nd-order accuracy. In the range of the Reynolds number listed, it seems that δ should be about 0.005 in the above equation, i. e.,

$$\Delta_{min}=\frac{0.005}{\sqrt{R_e}}$$

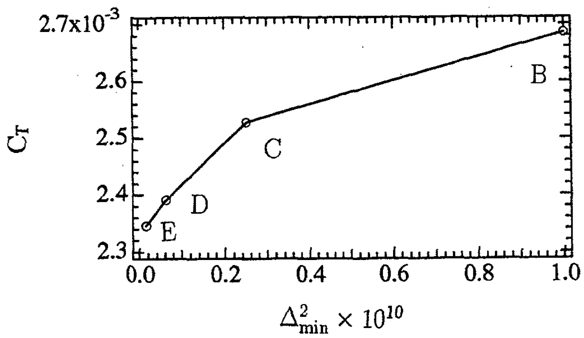

Fig. 5 Total drag C_T of flatplate vs. Δ^2_{min}. $Re=4.0\times10^7$

Table 3 Computed drag of a flat plate. Part 2...computation parameters. $R_e=4.0\times10^6$. Other parameters are common with Table 2.

Grid	r_{cl}	Inviscid term	Viscous term	$C_T\times10^2$
B	0.3	NU	V2	0.3331
〃	〃	U	〃	0.3331
〃	〃	NU	V1	0.3330
B_2	0.1	〃	V2	0.3330

, ten times smaller than that in previous computations, in order to compute the drag within 1% convergence (with respect to grid resolution) error. The converged C_T values are slightly smaller than the Schoenherr vaues.

Table 3 shows the cases $R_e=4.0\times10^6$ with various accuracy of the differencings. The NU and U differencings were used in the inviscid terms, and V1 and V2 were used in the viscous terms. Further, the effect of the change in the clustering ratio γ_{cl} was tested, since the wall shear stress changes very rapidly at both the edges, as shown in refs. 2) and 9). The V1 and V2 produced the same C_T value, which seem to suggest that the grid points are well within the viscous sublayer, where the velocity has linear distribution. The fact that NU and U produced the same C_T value is supported by the fact that there is only frictional (viscous) component in this drag.

4. Series 60 (C_B=0.60) Hull

Computations were made for the Series 60 (C_B=0.60) hull in the Reynolds number range $R_e=4.0\times10^5$ to $4.0\times$

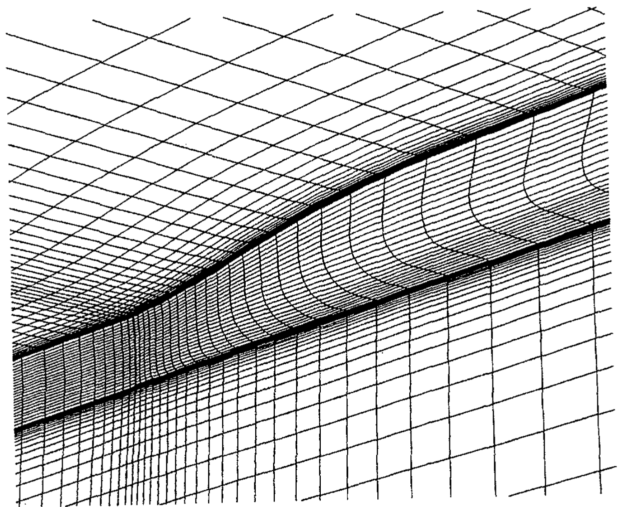

(a) Bow

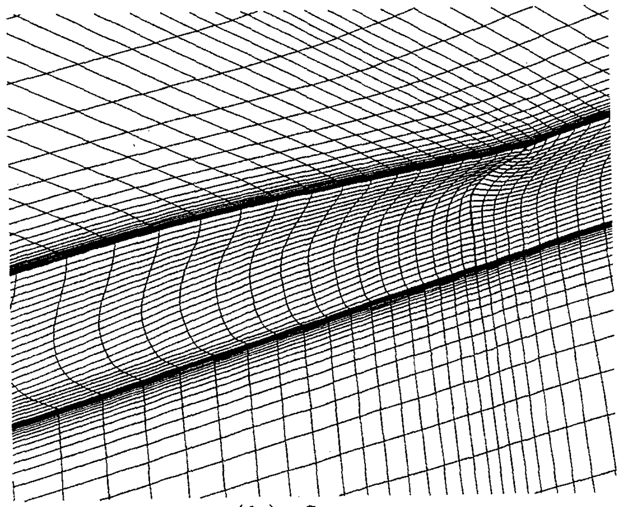

(b) Stern

Fig. 6 Grid B of Series 60 hull.

NII-Electronic Library Service

10^7.

The grid was generated using the implicit geometrical method[5]. Fig. 6 (a), (b) show the grid near bow and stern. The grid points are clustered toward bow and stern. Table 4 shows the computation parameters. Initially the flow is uniform everywhere. Computations were made using $\Delta t=0.01$ in most cases except the first 40 or 50 steps, in which Δt was made much smaller. With $\Delta t=0.01$ the nominal Courant number becomes 4,000 in the smallest $\Delta_{\min}$ grid. Computations were carried out up to the nondimensional time of approximately ten. Then the drag integrated at the outer boundary agrees well with that at the ship hull, although no strict criterion for convergence was taken. In order to simulate the effect of studs (turbulence stimulators) used in experiments, the flow was assumed laminar up to the point 5% from the bow ($x=0.05$), and thereafter the eddy viscosity was added.

Fig. 8 shows the wake contours at AP ($x=1.0$), compared with the measurements[10]. Althoug the overall agreement is reasonable, the computed result fails to predict the bulge of the boundary layer at the center. But this bulge is partly due to the propeller hub on the model ship, not present in the computed hull.

Fig. 8 shows the computed pressure contours at $R_e=4.0\times10^6$ using the grid B (case 6). At the bow (Fig. 8 (a)), the presure suddenly rises, and this causes slight oscillation in the streamwise direction. At the stern (Fig. 8 (b)), there is pressure recovery. The highest presure point in the stern is located slightly aft of the stern end.

The table 4 also shows the computed total drag coefficient C_T as a function of the minimum spacing $\Delta_{\min}$. C_{fric} is the frictional component, and C_{pres} is the pressure component. The same data is plotted in Fig. 10.

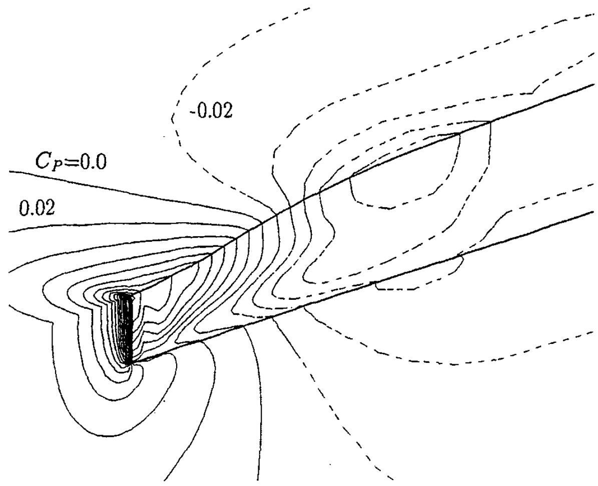

(a) Bow

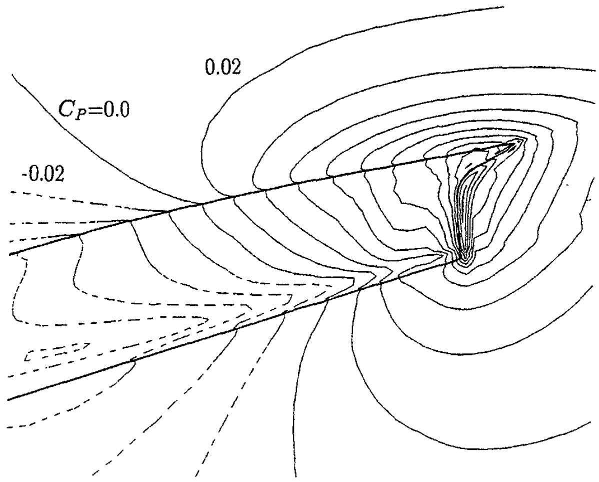

(b) Stern

Fig. 8 Pressure contours. Case 6 ($Re=4.0\times10^6$, Grid B)

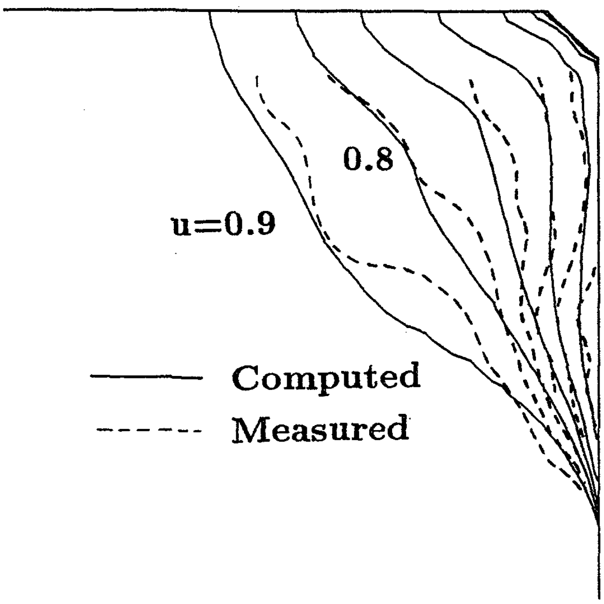

Fig. 7 Wake contours at Ap ($x=1.0$) section. Case 6 ($Re=4\times10^6$, Grid B)

Table 4 Computed drag of Series 60 ($C_B=0.60$) ship hull. Part 1... minimum spacings
Parameters: IM=81, JM=25, KM=41, I_{FP}=16, I_{AP}=60, $R_{outer}=1.0$, $x_{up}=-0.5$, $x_{down}=2.0$, $\gamma_{c1}=0.3$, $\beta=1.0$, NU, V2, SM, $\Delta t=0.01$.

Grid	R_e / Δ_{min}	No.	4×10^5	No.	1×10^6	No.	4×10^6	No.	1×10^7	No.	4×10^7
A	2×10^{-5}	1	0.5995 0.5502 0.0493 1.132	-	$C_T\times10^2$ $C_{fric}\times10^2$ $C_{pres}\times10^2$ 1 + K	5	0.3869 0.3541 0.0328 1.130	-	—	12	0.2615 0.2369 0.0246 1.106
B	1×10^{-5}	2	0.6049 0.5566 0.0483 1.143	4	0.4917 0.4522 0.0395 1.115	6	0.3786 0.3473 0.0314 1.106	11	0.3360 0.3076 0.0285 1.145	13	0.3037 0.2771 0.0265 1.284
C	0.5×10^{-5}	3	0.6216 0.5739 0.0477 1.174	-	—	7	0.3837 0.3532 0.0305 1.121	-	—	14	0.2905 0.2659 0.0245 1.228
D	0.25×10^{-5}	-	—	-	—	-	—	-	—	15	0.2745 0.2524 0.0222 1.160
Schoenherr $\times10^2$			0.5294		0.4409		0.3423		0.2934		0.2365

The Society of Naval Architects of Japan

They show clearly that C_T decreases as the Reynolds number increases. At constant Reynolds number, in contrast to the flat plate result, the dependence of C_T on the minimum grid spacing Δ_{min} is not very clear, although at $R_e=4.0\times10^7$ C_T tends to decrease as Δ_{min} decreases. This phenomenon is also observed in the flat plate case. The same is true with the frictional component C_{fric} and the pressure component C_{pres}. This is perhaps due to the complex viscous and inviscid interaction in fully 3D flow. One cannot see any clear dependence of the form factor $1+K$ on the Reynolds number.

Table 5 shows the results using various differencing formulas. In the case 8, the upwind differencing U was used. C_{fric} remained unchanged, but C_{pres} increased by 20%. Since the change was only with the inviscid terms, that should influence only the inviscid component, i. e. C_{pres}. The case 9 shows the influence of the smoothing of the eddy viscosity ν_t. It turns out that the smoothing of ν_t causes little influence. The case 9 was computed with $\Delta t=0.01$, which means that the non-smoothing did not cause any degradation in numerical stability in this case. The case 10 shows the influence of the clustering ratio γ_{cl} toward bow and stern. Since, as shown in Fig. 8, there is a high and steep pressure peak at the bow, different grid resolution may cause significant change in C_{pres}. C_{fric} may also change significantly, because most of the contribution comes from the bow area, where the boundary layer is very thin. But it turns out that the change is very small. This is perhaps due to the global conservation property which the present scheme posesses.

Table 5 Computed drag of Series 60 ($C_B=0.60$) ship hull. Part 2...computation parameters. $R_e=4.0\times10^6$. Other parameters are common with Table 4.

No.	Grid	r_{cl}	Inviscid term	Smoothing of ν_t	$C_T\times10^2$	$C_{fric}\times10^2$	$C_{pres}\times10^2$
6	B	0.3	NU	SM	0.3786	0.3473	0.0314
8	〃	〃	U	〃	0.3849	0.3473	0.0376
9	〃	〃	NU	NSM	0.3784	0.3469	0.0315
10	B_2	0.1	〃	SM	0.3768	0.3477	0.0290

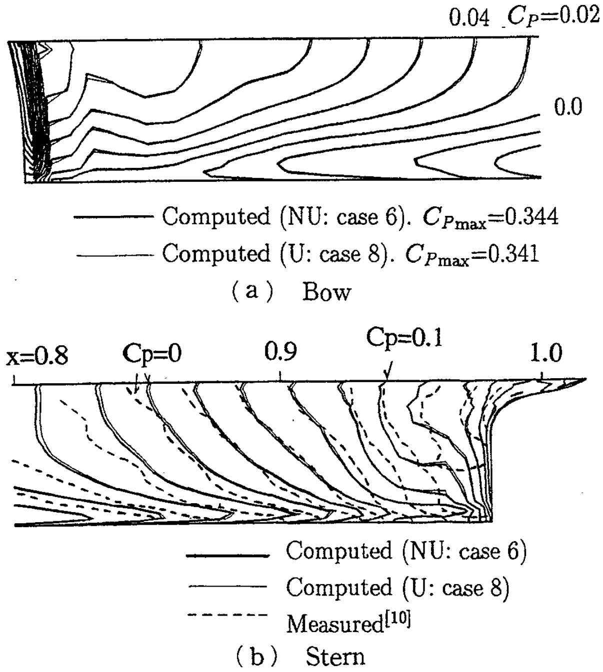

Fig. 9 Comparison of measured and computed pressure contours at stern. Cases 6 and 8.

Fig. 9 shows the pressure contours on the ship hull in the cases 6 and 8. Throughout the hull surface, the contours of the case 6 are located slightly upstream of those of the case 8. Considering the fact that the maximum pressure at the bow remains essentially the same, it is clear that this seemingly very small difference has caused the difference in C_{pres} by as much as 20%. This shows how sensitive the integration of C_{pres} is. Fig. 9(b) also shows the comparison with measurements. The agreement with the computed values is good. The discrepancy at the stern end is due to the propeler hub present with the experimental ship.

Assuming that the results with minimum Δ_{min} are the best ones, C_T and C_{fric} in the cases 3, 4, 7, 11, and 15 are plotted in Fig. 11, together with the measured values[11]. The measurements were made in towing tanks. In order to avoid the wave effect, only the values at smaller Froude numbers, say less than 0.23, were plotted. The agreement of the computed values of C_T with the measurements are very good in all the Reynolds number range computed. The Shoenherr line is also plotted. C_{fric} is consistently slightly larger than the Schoenherr value. This may suggest that the form factor comes not only from the pressure component but also from the frictional component.

Having good agreement in Fig. 11, the validity of CFD for computing the drag of a ship hull with sufficient accuracy using a reasonable amount of grid points, has thus been established.

Acknowledgments

The author thanks members (Dr. K. Nozawa of the

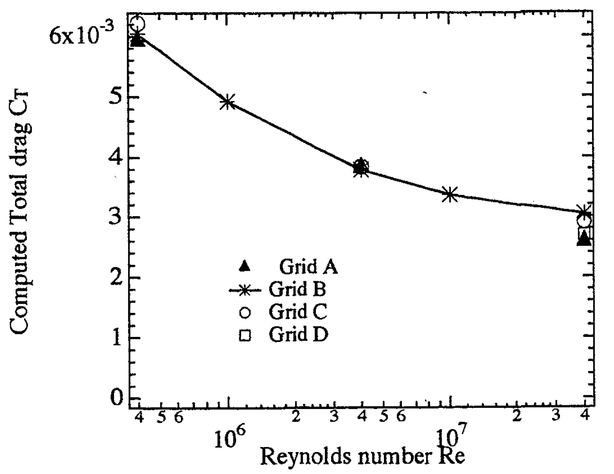

Fig. 10 Computed total drag C_T vs. Reynolds number.

NII-Electronic Library Service

The Society of Naval Architects of Japan

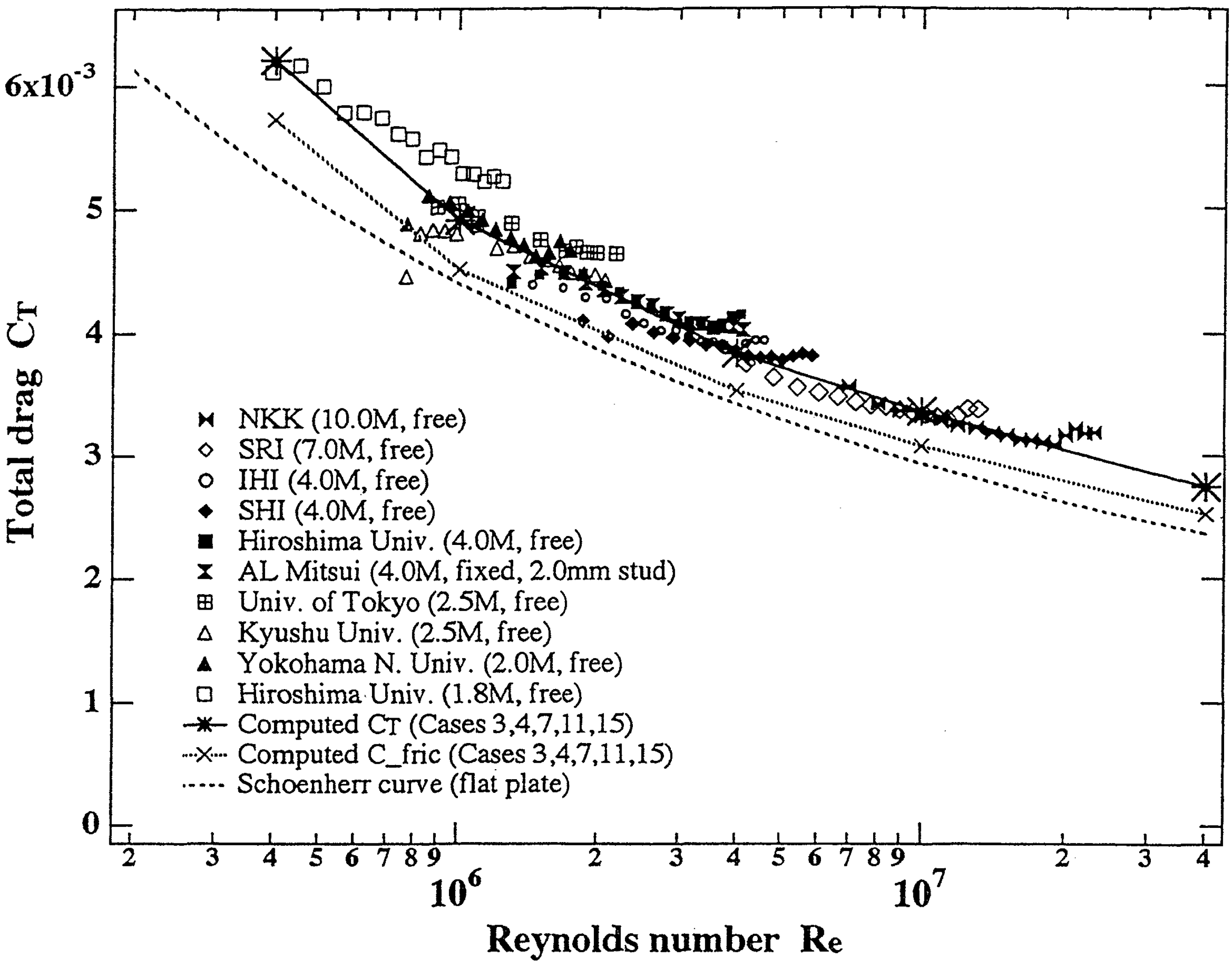

Fig. 11 Comparison of measured and computed total drag of Series 60 hull.

Kawasaki Heavy Industries Ltd., the manager) of the cooperative CFD research program between shipbuilding companies (HZ, IHI, KHI, MES, MHI, NKK, and SHI) and the Ship Research Institute for many test computations and valuable discussions on the acuracy of the computational scheme.

References

1) Kodama, Y. "A Cell-centered, Finite-Volume Upwind Scheme wih Global Conservation", J. of the Society of Naval Architects of Japan, vol. 168, December 1990, pp. 21-30.
2) Kodama, Y. "A Finite volume, Upwind Scheme with Global Conservation for Incompressible Flows", Proceedings of the 8th NAL Symp. on Aircraft Computational Aerodynamics, NAL SP -14, November 1990 (In Japanese).
3) Kodama, Y. "A Globally Conservative Upwind Scheme Applied to Flow past a Ship Hull", Proceedings of the 2nd Osaka Int. Colloquium of Viscous Fluid Dynamics in Ship and Ocean Technology, 1991, pp. 171-185.
4) Kodama, Y. "CFD at the Beginning of Practical Use", 58th General meeting of SRI, December 1991, pp. 33-42 (in Japanese).
5) Kodama, Y. "Grid Generation around a Practical Ship Hull Form Using the Implicit Geometrical Method", J. of the Society of Naval Architects of Japan, vol. 169, June 1991, pp. 27-38.
6) Chakravarthy, S. R. and Ota, D. K. "Numerical Issues in Computing Inviscid Supersonic Flow over Conical Delta Wings", AIAA Paper 86-0440, 1986.
7) Chakravarthy, S. R. "The Versatility and Reliability of Euler Solvers Based on High-Accuracy TVD Formulations", AIAA Paper 86-0243, 1986.
8) Sawada, K. and Takanashi, S. "A Numerical Investigation on Wing/Nacelle Interferences of USB Configuration", AIAA Paper 87-0455, 1987.
9) Kodama, Y. "Grid Generation and Flow Computation for Practical Ship Hull Forms and Propellers Using the Geometrical Method and the IAF Scheme", 5th Int. Conf. on Num. Ship Hydro., 1989.
10) Toda, T. et al. "Mean Flow Measurements in the Boundary Layer and Wake of a Series 60 C_B=0.6 Model", IIHR Report No. 326, 1988.
11) ITTC Cooperative Experiments on a Series 60 Model (CES-60), organized by the Resistance and Flow Committee, 18th ITTC, 1987.

NII-Electronic Library Service